Macromolecules

pubs.acs.org/Macromolecules Article

Thermal Transport in Polyethylene: The Effect of Force Fields and Crystallinity

Sandra Sæther, Merete Falck, Zhiliang Zhang, Anders Lervik, and Jianying He*

Cite This: *Macromolecules* 2021, 54, 6563–6574 Read Online

ACCESS | Metrics & More | Article Recommendations | Supporting Information

ABSTRACT: In this article, we study the local structure and heat transfer properties (thermal conductivity and interfacial conductance) in model semi-crystalline polyethylene (PE) by non-equilibrium molecular dynamics. We compare three different force fields with different levels of detail (all-atom, all-atom with constraints, and united-atom) and find that the structure of the model PE is significantly influenced by the choice of force field. The united-atom force field results in a reduced overall crystallinity and an over-idealized organization of the polymer chains, compared to the all-atom force fields. We find that thermal transport properties are not greatly influenced when structural effects are taken into consideration, and our results suggest that united-atom models can be used to study heat transfer properties of model PE, with decreased computational cost.

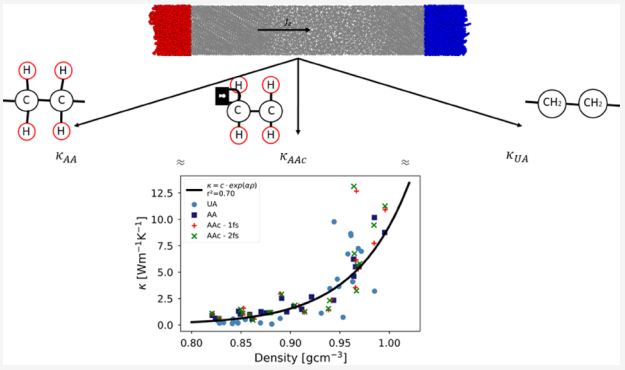

1. INTRODUCTION

Polymers are widely used materials that have many important applications in packaging, electronics, and thermo−electric devices due to their many beneficial properties, such as being lightweight, inexpensive, stable, and nontoxic. However, due to the low thermal conductivities of purely amorphous polymers, typically between 0.1 and 0.5 W m^{-1} K^{-1},[1] they have poor heat transport properties. This leads to challenges when polymers are used in microelectronic devices, as Joule heating leads to accumulated heat due to the difference in thermal conductivity between the polymer and other parts of the circuit, typically metals. Examples of strategies in place to improve the thermal conductivity of polymers includes filling the polymer with highly conductive particles or aligning the polymer chains. Since the thermal conductivity of a polymer is high along its backbone, the latter approach has for polyethylene (PE) resulted in nanofibers with thermal conductivities of around 100 W m^{-1} K^{-1},[2] approaching the recently estimated theoretical limit of PE crystals (164 W m^{-1} K^{-1}) .[3] Microfibers of PE with a thermal conductivity of around 60 W m^{-1} K^{-1} have also been developed .[4] Fibers have some practical drawbacks for applications and an alternative is therefore films.[5] Recently, Xu et al. developed a PE film with a thermal conductivity of 62 W m^{-1} K^{-1}.[6] All of these constructed structures consist of structural anisotropic semi-crystalline PE.

To understand the thermal transport in PE on an atomistic level, molecular dynamics (MD) simulations have been widely utilized. One of the most prominent successes was the prediction of high thermal conductivities of PE,[7] which was later confirmed by experiments.[2] Since then, a substantial number of MD simulations have been performed[5,8−12] to investigate the thermal transport in PE and to understand what affects it. However, the different studies use systems that are often either purely crystalline and focusing on single chains[8,11,12] or purely amorphous.[10] While they all give valuable insights into how the different morphologies contribute to heat transfer, these systems do not represent the polymers in use in most practical applications, as more than 60% of industrial plastic is in the semicrystalline state.[13]

In addition to having idealized PE systems, little focus has been put on quantifying the effect of the degrees of freedom in the force fields used in MD studies of the heat transfer in model PE. Some studies use united-atom (UA) force fields,[5,10,14,15] while others use all-atom (AA) force fields.[11,12] Different thermal conductivities have been reported in the literature for the same polymer system when different degrees of freedom are employed.[16−20] Algaer and Müller-Plathe studied the thermal transport in polymers with MD simulations and suggested adding bond constraints to remove fast degrees of freedom and avoid overestimation of thermal conductivities.[16] Lussetti et al.[17] found similar results for the thermal conductivity of amorphous polyamide-6,6, where the

Received: March 21, 2021
Revised: June 9, 2021
Published: June 25, 2021

https://doi.org/10.1021/acs.macromol.1c00633
Macromolecules 2021, 54, 6563−6574

thermal conductivity increased with the number of degrees of freedom in the system, and they concluded with a UA force field being the best approach. They reasoned that this is due to the fast vibrations of hydrogen atoms artificially contributing to the thermal transport. The same trend of thermal conductivity increase with increasing degrees of freedom has also been found for water[18] and other molecular liquids.[20]

However, when this was tested for crystalline syndiotactic polystyrene, no systematic variation of the thermal conductivity with the degrees of freedom was found.[19] As pointed out by Rossinsky et al., constraints involving the backbone of the polymer chain will always lead to a significant reduction of the thermal conductivity in the polymer system, as these bonds are responsible for most of the heat transport along the polymer chain. As the study by Lusetti et al. mostly involved these types of constraints, the trend found by this study is not surprising. In the study of syndiotactic polystyrene, however, pendant groups and atoms were tested, and adding constraints to these groups did not give the same effect, as they mainly contribute to the thermal transport by the less efficient energy transfer of collision.

Other sources of errors that could give rise to the difference in thermal conductivities predicted by these methods are the difference in force constants utilized, as the thermal conductivity obtained depends greatly on this. Further, if the harmonic approximation is utilized for the bonds, the thermal conductivity should not be calculated for elevated temperatures.

Whether the structures and dynamics of polymer structures produced by AA and UA force fields are comparable to each other, and to experimental results, have been the study of several papers. Chen et al. compared AA, UA, and coarse-grained models of poly(ethylene oxide), and could find no clear evidence that the AA model provided a better description than the UA model.[21] This was also investigated for poly(methyl methacrylate), where it was found that the AA model better resembled the dynamics of the experimental data, but the UA model provided a reasonable approximation. They note that in order to properly study the entire dynamic range, a combination of different descriptions is required.[22] A study by Li et al. looked at the effect of AA and UA on chain folding for PE and found that this had a noticeable impact on the structure of the lamellar, where the AA model had non-uniform foldings of the chains while the UA model had tightly aligned, folded chain segments.[23] They conclude that, regardless of the potential used, UA models yield structures folded in ways significantly different from the AA models.

From the discussion above, it is expected that the force field employed in MD simulations of PE systems will influence both the structure and heat transfer properties. UA force fields seem to generally be better at modeling heat transfer properties (by removing the hydrogen degrees of freedom), compared to AA force fields, with the added benefit of being computationally less expensive. However, the use of UA models may alter the structure significantly, which in turn will influence heat transfer characteristics. In particular, when studying models of semicrystalline PE for realistic industrial applications, the findings of Li et al.[23] suggest that the use of UA force fields can lead to the presence of unrealistic nicely folded, short lamellae as a consequence of the hydrogen−hydrogen repulsion lacking, making the *trans*-gauche rotation easily accessible. It is therefore not clear what impact the force field will have on heat transfer properties. To assess the impact of different degrees of freedom on the structure and thermal conductivity of PE, we have carried out systematic MD simulations of semicrystalline PE with three different force fields: AA, AA with constrained hydrogen bonds (AAc), and UA. Here, the degrees of freedom range from high (AA) to low (UA). By varying the degrees of freedom, we can discern the effect of structure on thermal conductivity.

The paper is structured as follows; in Section 2, the simulation models and methods are presented, and details of the data analysis used to characterize the systems are given in Section 3. In Section 4, the results are presented and discussed, and Section 5 contains the summary and conclusions of our study.

2. SIMULATION MODELS AND METHODS

To study the heat transfer in the different PE systems, we carried out boundary-driven non-equilibrium molecular dynamics simulations (NEMD),[24−26] where explicit temperature gradients are created in the system by thermostatting different regions in the simulation box. NEMD simulations have been widely used to calculate thermal transport properties for polymers[5,10−12,15,17,20,27] and can be applied to any system in the linear-response regime. The underlying assumption of equilibrium has to be fulfilled, which has been shown to be valid even at a high-temperature gradient and for a small number of particles in the control volume.[28] All simulations were carried out using the LAMMPS software.[29]

The force fields we have considered are based on the OPLS (optimized potential for liquid simulation) force field.[30] The OPLS force field was originally developed to reproduce thermodynamic properties of liquid- and gas-phase organic molecules and has been used successfully to reproduce thermal conductivities of polymers.[14] The interatomic interaction parameters were collected from Olsson et al.,[31] with references therein,[30,32,33] and are given in the Supporting Information (Tables SI-1 and SI-2), together with the non-bonded interaction parameters. In the present study, partial charges were set to zero, meaning that Coulomb forces were neglected. Previous studies have found that the effect of including the Coulombic forces have a negligible effect on the structure of PE.[31] The non-bonded interactions were truncated with a cut-off of 12 Å for all systems. For the AA system with constraints (AAc), hydrogen bonds were constrained using the SHAKE algorithm.[34] In the UA system, CH_2 and CH_3 fragments are represented as two unique beads.

2.1. Creation of Initial Semi-crystalline Systems. To represent the chaotic nature of real life polymers, we focused on semicrystalline polymer systems.

There are two main approaches to simulate semicrystalline polymer systems. The first is to construct the system to be semicrystalline from the start and arrange the polymer chains to have a layered structure of amorphous and crystalline phases, with a well-defined interface.[31,35,36] This is the strategy chosen by Lu et al. to study the effects of tails, bridges, and loops on thermal transport.[5] The second approach is the "amorphous melt" procedure, in which an amorphous polymer structure is equilibrated at a high temperature in order to explore the configurational phase space, and thereafter cooled down to enable crystallization.[37−41] It is however important to note that the cooling rates in MD simulations are higher than those in experiments due to time restraints, resulting in quenching of the structures. The first approach results in realistic lamellar stacks, whereas the second approach results in less organized structures, which may more closely resemble the natural, chaotic equilibration structure of polymers. We have therefore chosen to initialize our systems with the amorphous melt approach in this study.

Three AA PE systems with different initial configurations were prepared using the enhanced Monte Carlo (EMC) software.[42] Every system consisted of 250 PE chains containing 150 carbon atoms each, leading to a total number of 113,000 atoms. After creation, all systems were put through a thorough equilibration process. They were placed in a large simulation box with $(x \times y \times z)$ dimensions of 100 × 100 ×

https://doi.org/10.1021/acs.macromol.1c00633
Macromolecules 2021, 54, 6563−6574

279 Å and heated up to 900 K. The *NVT* ensemble (with a Nose–Hoover thermostat as implemented in LAMMPS) and a timestep of 1 fs were used, with periodic boundary conditions in the x and y dimensions and a fixed boundary in the z dimension. After 10 ns at this temperature, the temperature was set to decrease to 500 K during a 10 ns run, before continuing the step-wise cooling to 400 K over an additional 10 ns run. The systems were then compressed in the x- and y-dimensions to reach a density of minimum 0.85 g cm^{-3} during a 10 ns run at 400 K. For two of the systems, a compression in the z-dimension was also performed. After this compression, the systems were cooled to 315 K during a 10 ns run, before a final 10 ns *NVT* simulation at 315 K. The minimal run time was 51 ns for this equilibration process. In order to ensure that the systems were stable, the radius of gyration and total energy of the systems were monitored during the final *NVT* run (see Supporting Information 5.1).

The UA systems were created from the equilibrated AA systems by extracting the positions of the carbon atoms in the AA systems and converting them to CH_2 or CH_3 beads. The resulting UA systems were then allowed to expand by placing the structure in an enlarged simulation box (10 Å larger in each dimension), where it was run at 315 K for 10 ns in a *NVT* simulation, before the same density criterion was applied. After this, the UA systems were equilibrated for a minimum of 25 ns at 315 K in a *NVT* simulation.

This process resulted in three stable semi-crystalline systems, which will be referred to as system 1, system 2, and system 3 in the following. Since each system have AA, AAc, and UA representations, the system names will be suffixed with AA, AAc, or UA to distinguish them, for example, "system 1–AA".

2.2. Non-equilibrium Molecular Dynamics Simulation of Heat Transfer. After the equilibration process, the thermostatting regions for the NEMD simulations were defined at the ends of the simulation box in the z-dimension, with a thickness of ∼20 Å. The temperature was set to T_c = 300 K at the cold side and to T_h = 325 K at the hot side, and two separate velocity rescale thermostats were used to control the temperature in these regions. The equations of motion were integrated using the velocity–verlet integrator as implemented in LAMMPS. The NEMD system setup is visualized in Figure 1.

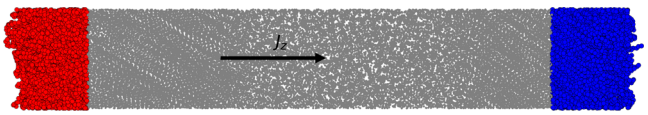

Figure 1. Representative picture of the NEMD simulation process. The PE chains are shown as spheres, and the atoms in the two thermostatted regions are colored as blue (cold region) and red (hot region). The direction of the heat flux is indicated with the black arrow.

Before a production run, the system under investigation was equilibrated with the thermostats turned on in order to reach a stationary state. The AA/AAc systems had an equilibration time of 15 ns before a stationary state was reached and then a 40 ns production run. For the AAc systems, the influence of the simulation timestep was investigated by running additional equilibration and production simulations with a timestep of 2 fs. The UA systems were subjected to a 100 ns equilibration run before a 100 ns production run. The UA systems did not need a longer equilibration, but this was done to have less noise in the data, as the UA systems have considerably fewer particles. Three independent production runs were made for each system, with different seeds for generating initial velocities corresponding to a starting temperature of 315 K.

3. DATA ANALYSIS

The production runs were analyzed in order to extract information about the density, crystallinity, orientation of the PE chains, and temperature profile of the three different polymer systems. To avoid correlation effects, the recorded data points were separated by a minimum of 10 ps (10,000 MD steps). The raw data from the independent runs were averaged, and the analysis was performed on the ensemble-averaged data. To investigate local properties, the systems were divided into 100 bins along the direction of the temperature gradient. Each bin contained a minimum of 1000 particles for the AA/AAc systems and a minimum of 340 particles for the UA systems.

3.1. Characterization of Structures. As the amorphous melt approach is utilized, the resulting structures need to be analyzed in order to classify regions as crystalline or amorphous, and to locate possible interfaces between them. In order to determine the crystallinity, three different approaches were used. The first approach was the two-phase model,[5] where the degree of crystallinity, χ_ρ, in the structure is quantified by its relation to the density of the system, ρ

$$\rho = \rho_\chi \chi_\rho + \rho_A(1 - \chi_\rho) \tag{1}$$

where ρ_χ = 1.0 g cm^{-3} and ρ_A = 0.86 g cm^{-3} are the densities of crystalline and amorphous PE.[5,43] The second approach was to look at the average density in the bins of the systems. If this density was larger than ρ_{frac} = 0.95 g cm^{-3}, which is the density of high density PE (HDPE),[43] the section was classified as crystalline. The total crystallinity is then found as a fraction of the number of crystalline bins over the total number of bins. The third approach was a local analysis of the 250 individual PE chains of each system, in which three criteria summarized in the Supporting Information (SI 2) were used to classify parts of a chain as crystalline or not. To study the structural organization of the chains in the direction of the heat flux, an orientational order parameter, S, was calculated as a function of the z-coordinate. This orientational order parameter is given by[44]

$$S = \langle \cos[2(\phi - \bar{\phi})] \rangle \tag{2}$$

where ϕ is the angle between $\mathbf{r}_{i-1,i+1}$ and the z-axis, $\bar{\phi}$ is the average of this angle as a function of z, and the average $\langle ... \rangle$ is calculated as a function of z.

3.2. Analysis of Heat Transfer Properties. In the stationary state, the thermal conductivity (κ) is found assuming that the heat transfer obeys Fourier's law. For a one-dimensional case with the heat transfer along the z-direction, as in our simulation setup, Fourier's law gives

$$\kappa = -\frac{J_q}{(dT/dz)} \tag{3}$$

where dT/dz is the temperature gradient along the z-direction and J_q the corresponding heat flux. The heat flux in the simulation is given by

$$J_q = \pm \frac{\langle E_{kin} \rangle}{\delta t \times A} \tag{4}$$

where $\langle E_{kin} \rangle$ is the ensemble average of the kinetic energy added (+) to the cold thermostat or subtracted (−) from the hot thermostat, δt is the simulation time step, and A is the cross-sectional area perpendicular to the heat flux. In order to find the heat flux for a system, the cumulative kinetic energy added (or subtracted) for all of the simulation runs were plotted against the simulation time, and the average kinetic energy added (or subtracted) per time step was obtained from a linear least squares fit.

https://doi.org/10.1021/acs.macromol.1c00633
Macromolecules 2021, 54, 6563–6574

The temperature gradient, dT/dz, in a system was obtained from the mean temperature profile (averaged over a full production run). This average was fitted with linear least squares regression in order to obtain the gradient and an overall thermal conductivity of the system. To gain a deeper understanding of the changes in thermal transport properties throughout semi-crystalline systems, the mean temperature profile from a production run was also fitted with linear least squares regressions in different regions. This was then used to find local temperature gradients and thermal conductivities. Between regions of different crystallinities, the thermal transport can also be interpreted in terms of an interfacial thermal conductance, G, given by

$$G = \frac{J_q}{\Delta T} \tag{5}$$

where ΔT is the temperature jump across the interfacial region. The location of such interfacial regions and the size of the accompanying temperature jumps were determined using the average angle $\bar{\phi}$, as peaks of this average angle correspond to sharp changes in orientation. These peaks were located using SciPy's[45] signal analysis. After locating the regions, the surrounding temperature data of the two different phases were fitted by linear least squares regression, and the temperature difference ΔT was found as the difference between the two last data points in these fittings.

The uncertainties in the thermal conductivities and the interfacial conductances were estimated as described in Supporting Information 3.

4. RESULTS AND DISCUSSION

4.1. Characterization of Structures. The crystallinities of the systems created are summarized in Table 1. Here, only the results for AAc (2 fs) are shown. The results for AAc (1 fs) are very similar AAc (2 fs) and can be found in the Supporting Information (SI 5.3). From this table, it is evident that the three methods used to evaluate the crystallinity of the systems in this study are in disagreement, especially for systems 1 and 3. For system 2, the methods are in agreement. By studying the AA and UA versions of the three different systems, visualized in Figures 2a,b, 3a,b, and 4a,b, the systems are obviously quite different, with system 2 resembling the lamellar super lattice structure seen in the polymer film created by Xu et al.,[6] while the other two systems have a more dispersed crystallinity for the AA force fields and clearly divided crystalline and amorphous layers for the UA force field. As the local analysis only considers the orientation of the chains throughout the system, it stands to reason that the analysis yields a higher degree of crystallinity for the AA systems than the two-phase analysis, as the chains are oriented, but might not be as densely packed as the crystalline PE density, ρ_χ, used in eq 1. The difference in crystallinity yielded by the two-phase model and the section fraction for systems 1 and 3 gives further insights into the structures and the differences between the AA systems and the UA systems. The two-phase model assumes that the whole system either consists of ideally crystalline parts or ideally amorphous parts, whereas the section fraction counts sections that have densities on the order of HDPE as crystalline. It can be seen that the two-phase model is too strict in this definition for the UA systems, as the density of even the most crystalline parts of this system does not reach a density of 1.00 g cm^{-3}, and as such, the predicted crystallinity for the UA systems increases from the two-phase model to the section fraction analysis. It can also be seen that the crystallinity for the AA systems decreases from the two-phase analysis to the section fraction analysis. This can be explained from the visualized structures, as the AA systems consist of a more dispersed crystallinity, leading to the overall density of the system to be high, but evidently not high enough for most of the sections to be considered crystalline according to the section fraction criteria.

Both the two-phase crystallinty analysis and the section fraction crystallinity analysis are dependent on the choice of $\rho_{\chi/\mathrm{frac}}$. The value of ρ_{frac} chosen for this study is smaller than the values used for pure crystalline phases; however, the value is within the range reported by Peacock for high density PE,[43] and the criteria agrees well with the visual representation of the chains. If ρ_{frac} is changed to 0.97 g cm^{-3}, we naturally see a decreased crystallinity. As an example, with this value, the crystallinity of system 3−UA decreases from 36.47% to 14.6%. In general, for these two systems, the local analysis gives a higher crystallinity for both the UA systems and the AA systems than the two-phase model (eq 1). The section fraction tends to give the lowest crystallinity for the AA systems, while the UA systems get a higher crystallinity from this approach than the two-phase model. In order to investigate this further, a nearest neighbor analysis was done on the carbon atoms (AA), or beads (UA), of the chains, and the results are color-coded in Figures 2a,b, 3a,b, and 4a,b. Four neighbors within 3.5 nm points to the carbon atom (bead) being a part of a crystalline PE orthogonal unit cell, and these beads are colored green. The rest are red. In comparing the AA systems with the UA systems, the amorphous regions of the AA samples have developed some degree of orientational order with more extended and aligned chains, while the UA amorphous regions consist of purely disoriented chains. This semi-structured amorphous phase found in the AA systems is normally observed experimentally after drawing a sample,[6] which is comparable to how the simulation systems were created. This might indicate that the structures created by AA force fields are closer to what is found in experiments. As noted by Li et al.,[23] due to a lack of the explicit hydrogen repulsion, the use of UA force fields can give rise to falsely nice folded, short lamella structures. However, for system 2, the same structure is seen for all systems. The AAc systems have the same structure as the AA systems and are included in Supporting Information 5.3.

Table 1. Overall Crystallinity for the Different Systems with Different Force Fields

system	force field	crystallinity (local analysis) (%)	crystallinity (two-phase model) (%)	crystallinity (section fraction) (%)
1	AA	55.53	43.30	35.30
	AAc (2 fs)	59.92	45.17	36.47
	UA	51.34	31.05	37.64
2	AA	51.67	52.05	51.16
	AAc (2 fs)	51.49	53.66	51.72
	UA	47.89	41.01	49.41
3	AA	55.24	33.94	10.59
	AAc (2 fs)	57.62	47.16	34.12
	UA	42.72	29.15	36.47

https://doi.org/10.1021/acs.macromol.1c00633
Macromolecules 2021, 54, 6563−6574

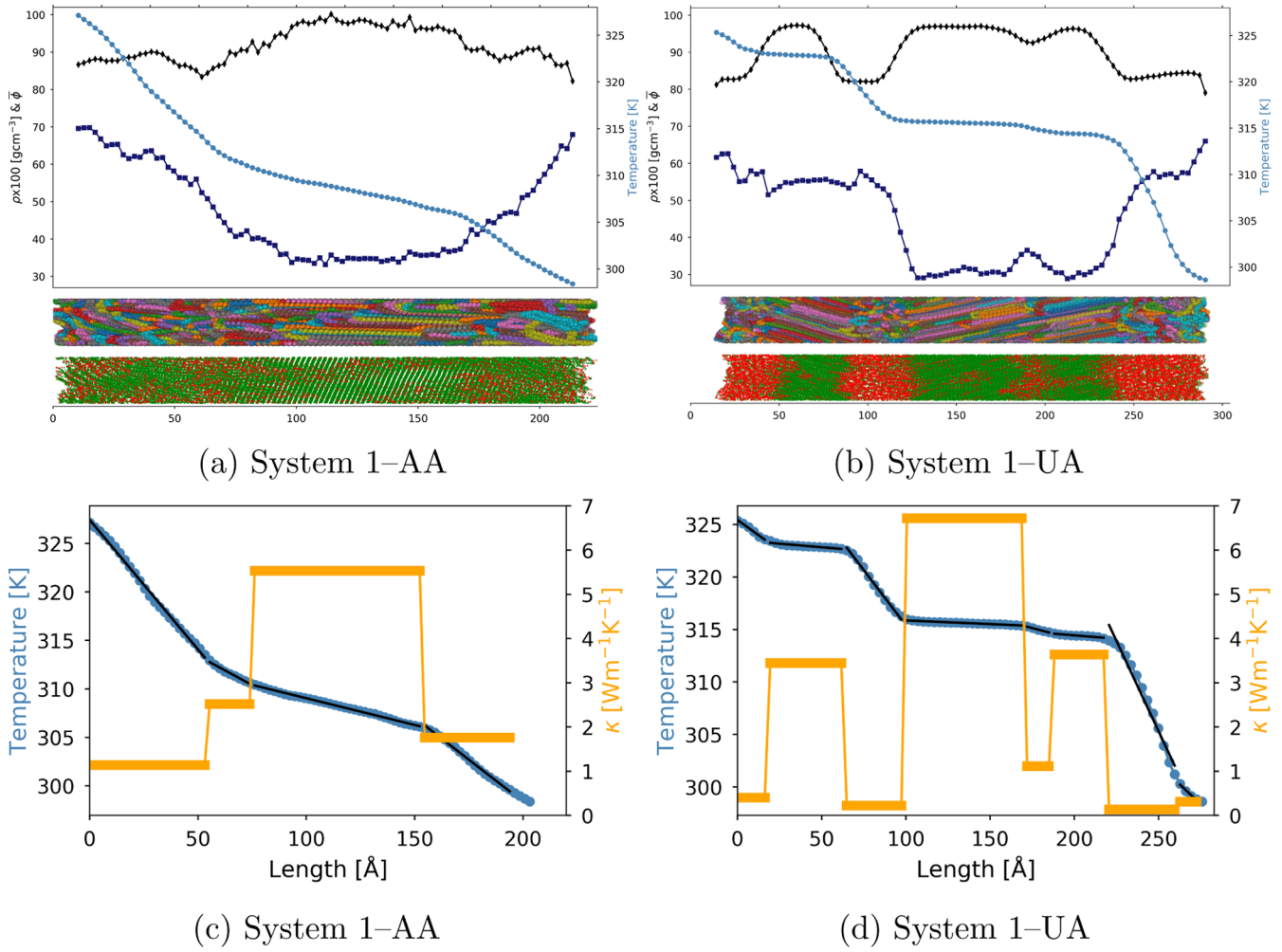

Figure 2. Structure and temperature profile for system 1. (Top) Scaled density (♦), average angle (■), and temperature (●) for system 1−AA (a) and system 1−UA (b). The individual polymer chains are shown in the lower part of the plot, together with the results from the nearest neighbor analysis where the particles are colored according to their number of nearest neighbors: 4 (green) or not 4 (red). (Bottom) The temperature profile of system 1−AA (c) and system 1−UA (d) fitted with linear regression in regions. The thermal conductivity in each region is approximated by the derivative of these linear fits.

After performing the analysis and visualizing the data, it was apparent that the order parameter S overlapped with the density, as can be seen from Figure 6b. This confirms that where the density is high, the chains are ordered, and therefore part of a crystalline lamellar. Visualizations of this are included in Supporting Information 5.2.

4.2. Thermal Conductivity. As a first overview of the thermal conductivity of the different systems, the overall thermal conductivity of each system was calculated by fitting a linear function to the full temperature profile. The temperature profiles across the systems are clearly not linear, as can be seen from Figures 2a,b, 3a,b, and 4a,b, but nevertheless this gives an estimation of the overall thermal conductivities of the systems, which is summarized in Table 2.

It is clear that within each system, the difference between AA and AAc is relatively small, and it is not possible to discern a single consequence of introducing SHAKE constraints: for system 1, the thermal conductivity of AAc is greater than for AA, for system 2, they are similar, and in system 3, AAc results in a thermal conductivity smaller than that of AA. This is in agreement with the study by Rossinsky and Müller-Plathe, where no systematic effect of introducing restrictions of degrees of freedom was found.[19]

There is a clear difference between the AA methods and the UA method, where a significant reduction in thermal conductivity is observed. As can be seen from Figures 2 and 4, the structures in system 1−AA and system 3−AA were not stable after conversion to UA, and they have changed drastically.

It is apparent from Table 2 that the different structures lead to different thermal conductivities: system 1 and 2 have comparable thermal conductivities, while system 3 is substantially lower. From the crystallinity analysis in Table 1, it can be concluded that system 2 has a higher thermal conductivity than system 3 due to a higher density (and overall crystallinity). For system 1 and 3, the crystallinity is similar, but the reason for the difference in thermal conductivity can be asserted from the orientation of the chains. The average tilt angle, $\bar{\phi}$, along the direction of heat transfer is lower for system 1 compared to system 3, meaning that the backbone atoms in the chains are oriented more in the direction of the heat flow for system 1, leading to higher thermal conductivity. This is

https://doi.org/10.1021/acs.macromol.1c00633
Macromolecules 2021, 54, 6563−6574

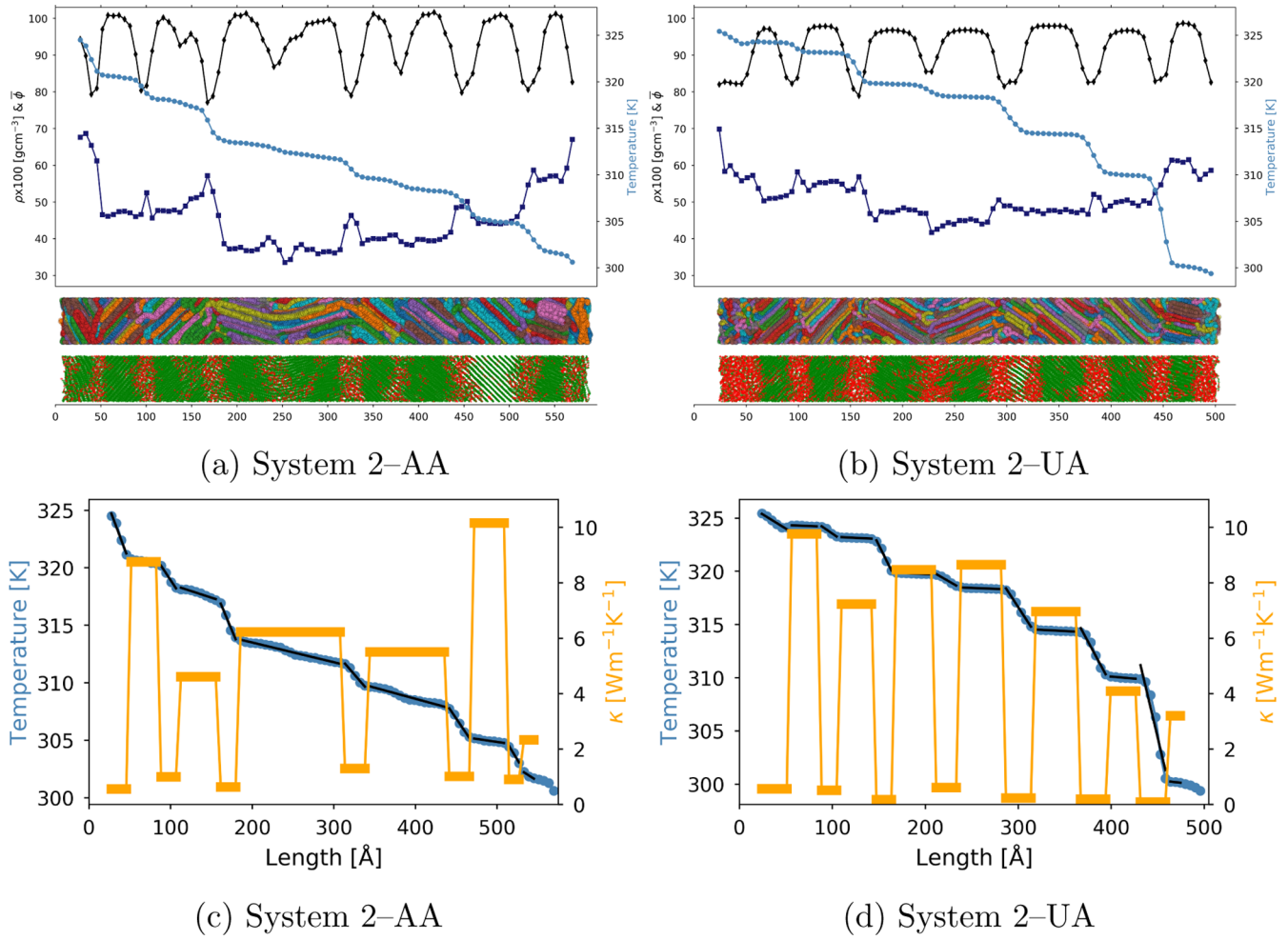

Figure 3. Structure and temperature profile for system 2. (Top) Scaled density (♦), average angle (■), and temperature (●) for system 2−AA (a) and system 2−UA (b). The individual polymer chains are shown in the lower part of the plot, together with the results from the nearest neighbor analysis where the particles are colored according to their number of nearest neighbors: 4 (green) or not 4 (red). (Bottom) The temperature profile of system 2−AA (c) and system 2−UA (d), fitted with linear regression in regions. The thermal conductivity in each region is approximated by the derivative of these linear fits.

also evident from the visualization of the chains themselves; see Figure 2a,b for system 1 and Figure 4a,b for system 3.

The structure of the PE systems changes quite drastically throughout the box. As previously mentioned, the overall temperature profile is not linear but instead consists of locally linear regions that can be fitted, as visualised in Figures 2, 3, and 4. This enables a study of how the local structuring of the chains affects the thermal transport. Two main factors influence the local thermal conductivity: local density and tilt angle. A high local density leads to highly aligned chains, and a low average tilt angle corresponds to the chains being mostly aligned in the direction of the heat flow, both leading to a higher local thermal conductivity. A low local density corresponds to an amorphous layer of the system, and higher tilt angles correspond to either an amorphous layer or chains being tilted away from the heat flow direction, both leading to a lower local thermal conductivity. By studying the structure of each system, it is therefore possible to understand why the thermal conductivities vary as they do. Taking system 1−UA as an example, the temperature profile can be divided into eight sections, as shown in Figure 2d. Here, the first part is purely amorphous, which is evident from the density, the visualization of the chains, and the nearest neighbor analysis, leading to a low local thermal conductivity. The second part is more ordered, with an eightfold increase in the thermal conductivity, but still with a relatively large tilt angle. The following part is amorphous again, classified by a drop in the density and increase of the tilt angle, leading to a significant reduction of the thermal conductivity. In the next phase, the local thermal conductivity is relatively high due to a lower tilt angle and higher density. After this, a small transition region emerges, with a more disordered structure, characterized by a peak in the tilt angle and a change in the number of nearest neighbors, before a more crystalline phase develops again, with a higher thermal conductivity. The local thermal conductivities range from 0.1 to 6.7 W m^{-1} K^{-1} for system 1−UA. This examination can be done for all the systems. The temperature profile of system 1−AA consists of four parts, as displayed in Figure 2c, with the local thermal conductivity varying from 1.1 W m^{-1} K^{-1} due to a lower density and higher tilt angle to 5.5 W m^{-1} K^{-1} due to highly aligned chains and a low average tilt angle.

System 2−AA and system 2−UA have a step-like temperature profile, with structures reminiscent of grain boundaries. Both have relatively low tilt-angles throughout the system, only broken up by several orientation changes where the density

https://doi.org/10.1021/acs.macromol.1c00633
Macromolecules 2021, 54, 6563−6574

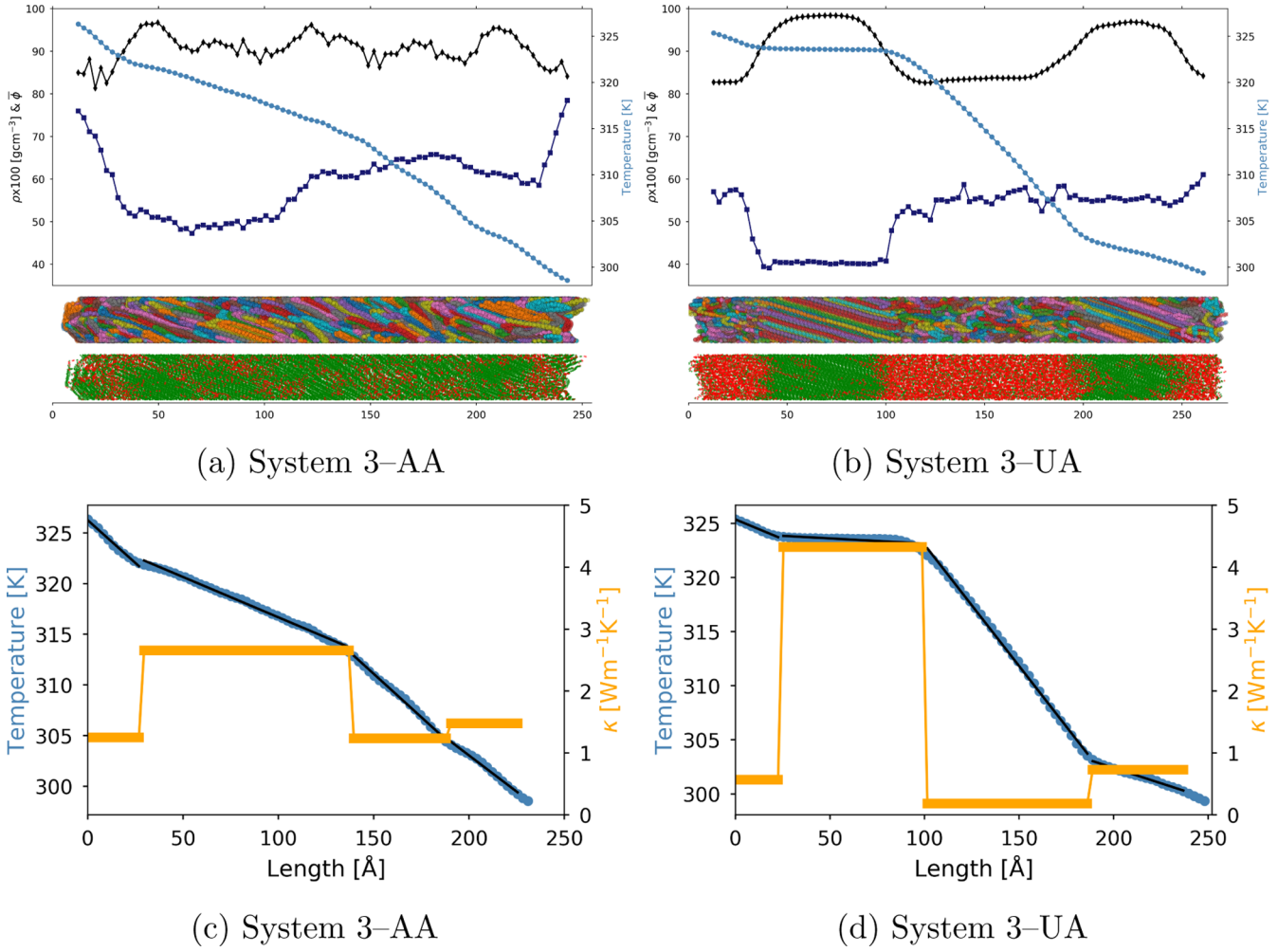

Figure 4. Structure and temperature profile for system 3. (Top) Scaled density (♦), average angle (■), and temperature (●) for system 3−AA (a) and system 3−UA (b). The individual polymer chains are shown in the lower part of the plot, together with the results from the nearest neighbor analysis, where the particles are colored according to their number of nearest neighbors: 4 (green) or not 4 (red). (Bottom) The temperature profile of system 3−AA (c) and system 3−UA (d), fitted with linear regression in regions. The thermal conductivity in each region is approximated by the derivative of these linear fits.

Table 2. Overall Thermal Conductivities for the Three Different Systems Given in W m^{-1} K^{-1}

	System		
force field	1	2	3
AA	2.471 ± 0.028	2.818 ± 0.071	1.750 ± 0.020
AAc (2 fs)	2.990 ± 0.028	2.862 ± 0.054	1.670 ± 0.014
UA	0.566 ± 0.015	0.512 ± 0.011	0.331 ± 0.005

drops, the number of nearest neighbors changes, and the thermal conductivity drops. This leads to high thermal conductivities in the range of 6−10 W m^{-1} K^{-1} for the crystalline areas. For the lower thermal conductivity areas, we can however note one difference between the AA and UA system. Although the AA system has a wider spread in the thermal conductivity of the more disordered parts, ranging from 0.6 W m^{-1} K^{-1} for the first section of the system to 2.3 W m^{-1} K^{-1} for the last section of the system, the UA system has consistently very low values for the disordered parts of about 0.05 W m^{-1} K^{-1}, which are clearly amorphous. It can also be seen that the disordered phases of the UA system are larger and more clearly defined than for the AA system, in which the phases have some degree of orientational order.

The same trend as for the two other systems can be seen for system 3, with the UA system being more strictly divided into purely crystalline and purely amorphous regions, whereas the AA system has a generally more ordered structure, but does not have any "ideal" crystalline parts. This is reflected in the local thermal conductivity, where UA has local thermal conductivities ranging from 0.6 to 4.3 W m^{-1} K^{-1}, whereas the AA system has local thermal conductivities ranging from 1.2 to 2.7 W m^{-1} K^{-1}. From Figure 4a, it is apparent that these differences in the local thermal conductivity does not stem from an increased ordering, but rather a difference in the average tilt angle.

The thermal conductivity results are summarized in Figure 5, where the local thermal conductivities are plotted against the density for all four methods and all three systems. By using all the data from our extensive study, an exponential curve for the local thermal conductivity as a function of density was fitted, resulting in an r^2 value of only 0.7, which makes it clear that the density alone cannot exclusively explain the thermal conductivity. This curve can however be used for qualitative comparisons between different force fields. The coefficients for this curve is given in Table 3. The first point of notice is that

https://doi.org/10.1021/acs.macromol.1c00633
Macromolecules 2021, 54, 6563−6574

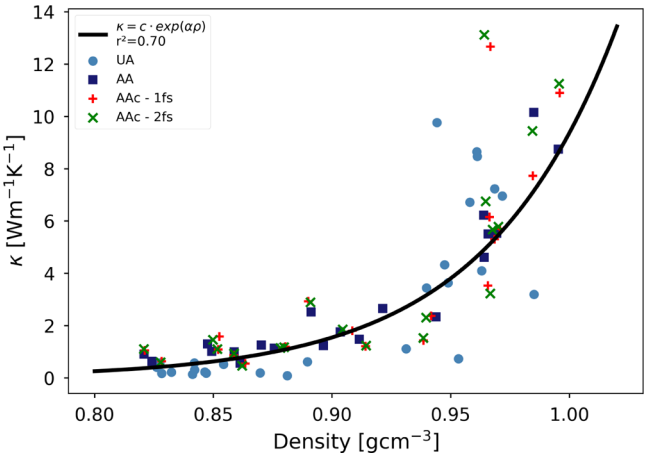

Figure 5. Local thermal conductivities of the different force fields, AA, AAc, and UA, plotted against the density. The fitted exponential curve has coefficients given in Table 3.

Table 3. Coefficients for the Curve Given in Figure 5

C	α
1.3894×10^{-7}	18.02760231

the density of the UA systems does not exceed 0.985 g cm^{-3}, even though it is evident from Figures 2b, 3b, and 4b that the chains are still crystalline and densely packed. This suggests that the density criteria for crystalline PE is different between the AA/AAc methods and the UA method. For the lower densities, around 0.85 g cm^{-3}, the local thermal conductivities of AA and AAc have slightly elevated values in comparison to UA at the same densities, but the methods agree reasonably well. For higher values, however, the local thermal conductivities of UA from around 0.95 to 0.98 g cm^{-3} have fluctuating values. It is therefore difficult to directly compare the values obtained from the UA system with the AA and AAc systems, and this is where the deviations from the fitted curve are clearly visible. The scattering in the data above 0.95 g cm^{-3} can to some degree be explained by the average tilt angle, $\bar{\phi}$.

As can be seen from Figure 6a, where the average tilt angle is plotted against the order parameter S, the tilt angle does not influence the local thermal conductivity for lower S values. However, when S reaches a critical value of >0.8, $\bar{\phi}$ has a clear effect on κ. This can easily be explained, as lower order parameters correspond to amorphous phases, where defining a tilt angle has little physical meaning. When the chains become more ordered, however, the tilt directly affects the thermal conductivity, and we see that for high order parameters of similar values, the local thermal conductivities are higher for smaller tilt angles than for larger. The largest value for κ obtained in this study, 13.122 W m^{-1} K^{-1} from system 2−AAc (2 fs), seems to deviate from this trend. This value does however correspond to the highest order parameter obtained in this study, of 0.956, and in addition belongs to a small area, which can contribute to some uncertainty in both the calculated thermal conductivity and the tilt angle. From Figure 6b we can see that the density and the order parameter have a linear relationship and that κ increases with both the density and the order parameter. A final point of notice is that the fitting of the curve could be improved by separating out the data for the UA systems and fitting them individually. However, as the goal of the study is to compare the methods, this is not done here. For the interested reader, these can be found in Supporting Information 5.4, in addition to the density *versus* the tilt angle plot for all of the data. From this, we conclude that the impact on thermal conductivity from restricting the degrees of freedom is less severe than it appears from a first glance at Table 2. These differences can be explained by the differences in the structures of the systems themselves since the UA systems have more well-defined amorphous parts and a higher number of interfaces, compared to the AA systems. For comparable subsections of the structures, the thermal conductivities are similar. It should also be noted that the local thermal conductivity of the amorphous sections in UA closely resembles experimental values of 0.4 ± 0.16 W m^{-1} K^{-1} for amorphous PE.[46] The overall thermal conductivity of the system 3−AA is in agreement with the value obtained by Muthaiah and Garg for aligned amorphous PE, with the COMPASS force field.[10] This is expected due to the resemblance of the structures. The value of the more ordered sections of both the AA and UA systems are harder to compare with other literature due to the non-ideal structures for some of the sections and the tilt angle. Experiments by Hansen and Bernier has shown that the thermal conductivity has a linear dependence on the density in the range from 0.96 to 0.99 g cm^{-3}.[47] This is not the same

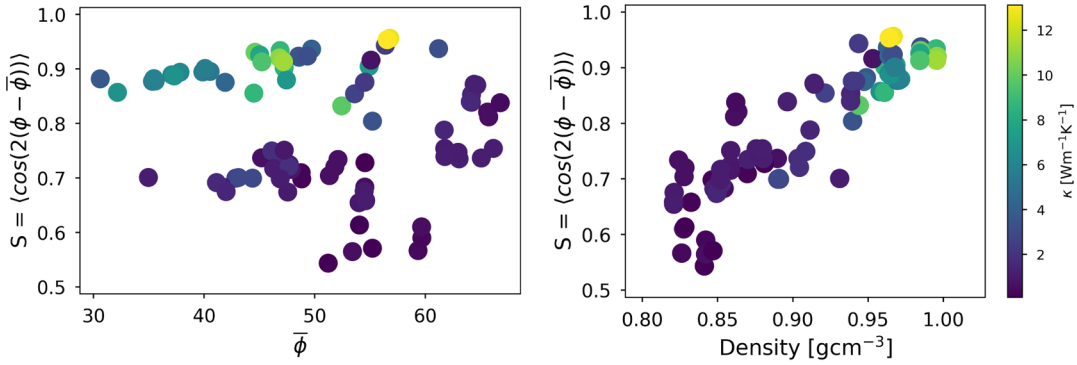

(a) The order parameter of the systems, S, plotted against the average tilt angle, $\bar{\phi}$.

(b) The density of the systems, ρ, plotted against the order parameter, S.

Figure 6. Order parameter is plotted against the average angle (a) and the density (b), with the points colored after their local thermal conductivity value.

https://doi.org/10.1021/acs.macromol.1c00633
Macromolecules 2021, 54, 6563−6574

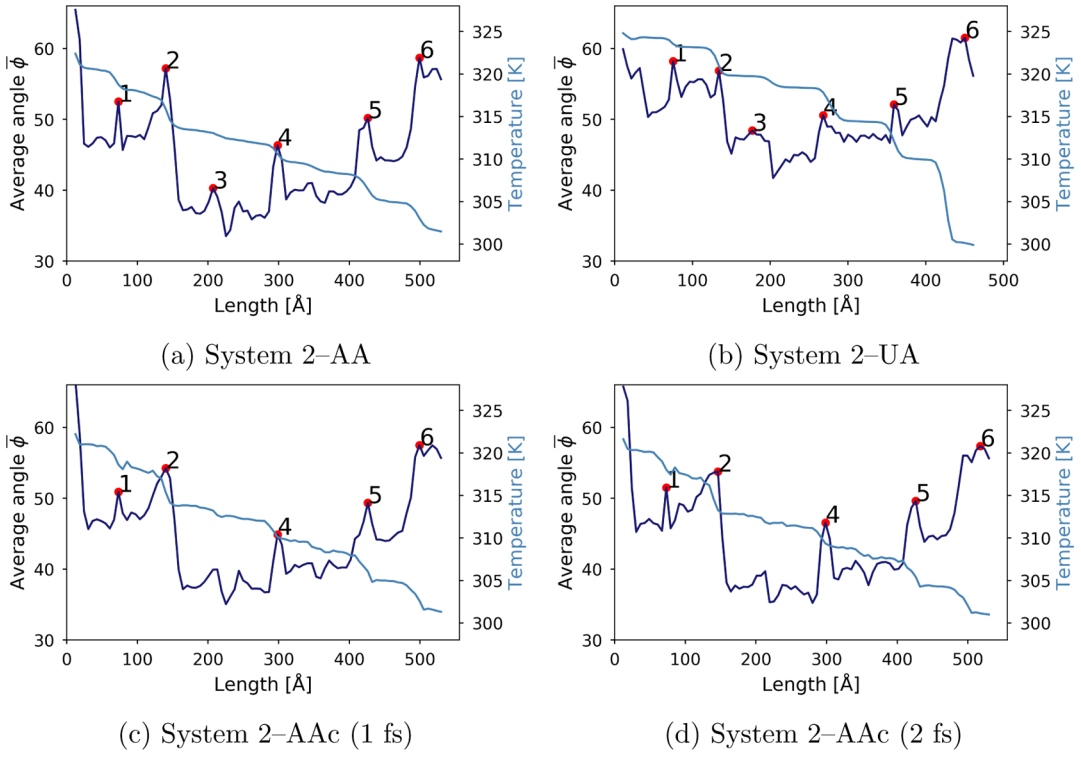

Figure 7. Average tilt angle, $\bar{\phi}$, (colored dark blue) and the temperature profile (colored blue) for system 2 as functions of the z-coordinate in the simulation box. The peaks of $\bar{\phi}$ are marked in red and numbered chronologically.

Table 4. Conductance Values (G) of the Interfaces Given in Chronological Order for System 2, as Illustrated in Figure 7.[a]

		1	2	3	4	5	6
AA	G	472.3 ± 0.21	327.5 ± 0.02	1408.5 ± 0.14	658.9 ± 0.06	371.2 ± 0.05	364.3 ± 0.05
	ΔT	2.26 ± 0.46	3.26 ± 0.07	0.76 ± 0.10	1.62 ± 0.10	2.87 ± 0.14	2.93 ± 0.15
AAc (2 fs)	G	542.2 ± 0.04	332.0 ± 0.03		608.9 ± 0.05	372.5 ± 0.03	635.3 ± 0.09
	ΔT	2.03 ± 0.09	3.32 ± 0.09		1.81 ± 0.09	2.96 ± 0.10	1.74 ± 0.09
UA	G	305.6 ± 0.17	96.9 ± 0.05	235.1 ± 0.40	80.2 ± 0.06	73.1 ± 0.04	32 ± 0.01
	ΔT	1.01 ± 0.17	3.19 ± 0.17	1.31 ± 0.53	3.85 ± 0.22	4.22 ± 0.17	9.64 ± 0.1

[a]All conductances are given in MW m^{-2} K^{-1}. In addition, the temperature drop (ΔT) associated with the interface is given in K

trend seen in our data for the same range in Figure 5. As their studies do not include PE samples with densities lower than this, it is not possible to compare the rest of the data. The values obtained for the thermal conductivities in their study were considerably lower than the values reported here, as they looked at bulk samples. However, they also studied samples deformed in a simple shear test, which gives similar structures as a cold tensile test. As previously noted, this is similar to how the systems were created. The thermal conductivity obtained from these samples are comparable to the values obtained for the overall thermal conductivities.

4.3. Interfacial Conductance. The structure of system 2 resembles a system with grain boundaries, where the chains are ordered in one direction with a given tilt in one section, bordering another section, where the chains are oriented with a different tilt. These changes are quantified by the change in the average tilt of the chains ($\bar{\phi}$), and, as is apparent from Figure 3, a peak of $\bar{\phi}$ corresponds to a drop in temperature and a change of orientation of the chains through an intermediate amorphous phase. These clear peaks of $\bar{\phi}$ can be used to locate interfacial boundaries. From a visual inspection of the tilt angle given in Figure 3, the peaks were required to have a minimum height of 39 for system 2−AA and system 2−AAc and 41 for system 2−UA. Additionally, the peaks were required to have a horizontal distance of 0.5 in order to avoid finding several smaller peaks for the same interface. After removing peaks in the thermostatted region, and combining peaks belonging to the same interface, the relevant peaks were located, as indicated in Figure 7, where the average tilt angle and the temperature profile in system 2 are shown as functions of the position in the simulation box. Here, the points belonging to the thermostated regions have been excluded, and the x-axis is shifted accordingly.

In order to find the interfacial thermal conductivities of the grain boundaries, the temperature profile prior to, and following, the drop was fitted with linear regression. This was used to define the temperature drop ΔT in eq 5. The interfacial thermal conductance calculated for the temperature drops defined in Figure 7 is summarized in Table 4.

As seen in Table 4, the AA/AAc (2 fs) systems have temperature drops ranging from 0.76 to 3.26 K, while system 2−UA have temperature drops from 1.01 to 9.64 K. This, in addition to the heat flux being vastly different in the two systems due to the difference in degrees of freedom carrying heat, leads to the thermal boundary conductance being very different for the two methods. Since the structures of the two

https://doi.org/10.1021/acs.macromol.1c00633
Macromolecules 2021, 54, 6563−6574

systems are not identical, the boundaries are not directly comparable. Still, some trends can be discerned: The first drop, marked as "1" in Figure 7b for UA, the fourth drop, marked as "4" in Figure 7a, for AA and AAc (2 fs), and the third drop ("3") for both AA and UA correspond to a small difference in the average tilt angle before and after the interface. This leads to smaller temperature drops and higher interfacial conductances. In the cases of drop "2", "5", and "6", for all systems, there are larger changes in the tilt of the chains, leading to a higher temperature drop and a lower thermal boundary conductance. One important difference is the thickness of the interfaces, as the UA structure has wider intermediate, amorphous areas in comparison to the AA structures. Integrating eq 3, for constant κ and J_q, eq 5 becomes $G = \kappa/|\Delta z|$, where κ is the (constant) thermal conductivity of the interface and $|\Delta z|$ is the thickness. Using this relation, we find that the κ values of the interfaces are comparable, which suggests that obtained differences in G stem from the difference in structures and not directly from the different degrees of freedom in the different force fields.

To further investigate the interfacial heat transport, we have computed the vibrational density of states for amorphous and crystalline systems. This was obtained as the power spectrum of the velocity autocorrelation function. From these spectra, we find that there are no large differences between intermediate amorphous and crystalline phases for the AA and AAc systems. For the UA system, however, the crystalline phase has more clear, well-defined peaks, whereas the amorphous layer has more scattering below 20 THz. This might also be a consequence of the UA system having clearly defined, large amorphous regions, in contrast to the AA and AAc systems' more intermediate states. The spectra obtained and the details of the procedure can be found in Supporting Information 4. The literature does not provide direct comparisons as the interfaces obtained in this study are not idealized cases. The thermal conductance of the interface between crystalline *n*-alkane chains have been calculated using a UA approach, where a value of ∼145 MW m^{-2} K^{-1} was obtained.[15] This thermal interfacial conductance was also studied by Zeng et al. using a UA approach, resulting in a value of 108 MW m^{-2} K^{-1} at 300 K.[48] As these works were used to study an interface between chain ends, they are not directly comparable to our case, where some chains extend throughout the interface. In the former cases, the conductance is controlled by van der Waals interactions, while the bonded interactions become important in the latter case. However, the effect of the tilt angle is also mentioned by Zeng et al. as having a potential effect on the thermal conductance, which is observed in this work.[48] The most direct comparison with our study is drop 1 for system 2−UA, where the chains are tilted with approximately the same angle before and after the interface, resulting in a thermal conductance of ∼305 MW m^{-2} K^{-1}. As the chains in this case are bonded, the thermal conductance should be higher. Drops 2, 4, 5 and 6 of system 2−UA all have a lower thermal conductance than this. This might be explained by the disordered chain structure. A study performed by Duan et al. looked at the effect of "kinks", that is, the existence of gauche states, in the PE chain on thermal conductance using an AA force field.[49] They predicted the absolute thermal conductance of an ideal, single chain to be 5200 MW m^{-2} K^{-1}, and the conductance of a single kink was found to be 2200 MW m^{-2} K^{-1}. Adding more kinks reduced the overall thermal conductivity of the chain. This effect is clearly seen in all of the systems in this study. As the chains all have multiple kinks, the heat transport throughout the systems is predictably lowered.

Other studies have explored interfaces involving PE interacting with other materials. In a study conducted by Hu et al., the thermal conductance of the interface between amorphous PE and Si and amorphous PE and diamond, both with and without interfacial bonding, was investigated using NEMD and an AA force field. They estimated the thermal conductance of the PE−Si interface to be 20 MW m^{-2} K^{-1} at room temperature, while the diamond−PE conductance was estimated to be 10 MW m^{-2} K^{-1}. With strong polymer−inorganic solid interfacial bonding, the conductance increases significantly, resulting in a thermal conductance of ∼100 MW m^{-2} K^{-1} for a Si−PE interface and ∼20 MW m^{-2} K^{-1} for a diamond−PE interface .[50] All of the interfacial conductances for system 2−AA are significantly higher than these values. This is expected, as the system tested by Hu et al. consists of amorphous PE and an interface, bonded or not bonded, between dissimilar materials. A study by Ni et al. explored the question of how high the interfacial conductance between PE and diamond can be under optimal circumstances and computed the thermal conductance for a system with completely aligned PE chains and an oriented single crystal diamond that are covalently bonded with the use of the reactive bond order potential. The thermal conductances obtained ranged from 690−930 MW m^{-2} K^{-1},[12] which is higher than some of the values obtained for system 2−AA. They explain this high thermal conductance with the perfect structure of the polymer and the covalent bonding to the diamond.

5. CONCLUSIONS

The simulations done in this study shows that the force field used to model polymers may have a significant influence on the structure. Constructing similar structures using AA and UA force fields poses challenges as the UA versions of the AA structures are not stable, and the UA structures will reorganize to form a stable configuration. From the resulting structures, it can also be seen that the AA force field more closely resembles the structures obtained in experiments, and the difference in structure is the largest for crystalline phases. In addition, no large amorphous phases were obtained for the AA and AAc systems. By visual inspection of the structures, and comparing with the three approaches for quantifying the crystallinity of the structures utilized in this study, it is clear that more than one method should be used: some small section of a system might have a high density, but consist of very short parts of chains and should therefore not be considered as crystalline, and likewise, chains may be organized, but not densely packed enough to be crystalline.

For the study of thermal properties, it is clear that all of the methods tested are comparable when structural differences are accounted for. The parts of the system where the structures are similar have similar thermal conductivities. This means that a UA force field can be used to find thermal conductivities, with a significant decrease in computational cost. In particular, this is useful for pure amorphous structures, which have similar structures in AA and UA force fields. We find that all force fields considered here result in an increased thermal conductivity for higher densities. For higher densities, the UA force field results in thermal conductivities that have larger variation and is lower than the AA methods. We suggest that

https://doi.org/10.1021/acs.macromol.1c00633
Macromolecules 2021, 54, 6563−6574

this is caused by sections with the same density having a different tilt of the PE chains.

Finally, we note that the thermal conductances of the interfaces between different phases in semicrystalline PE are generally large in comparison to interfaces between other materials. There is however a reduction in the thermal transport in comparison to chains in the same phase. As a result of this, the overall thermal conductance obtained from the systems created by the UA force field is lower than the systems created by the AA force field, due to larger interfaces in the UA systems.

■ ASSOCIATED CONTENT

Supporting Information

The Supporting Information is available free of charge at https://pubs.acs.org/doi/10.1021/acs.macromol.1c00633.

Force field parameters, structural characterization criteria, uncertainty calculations, vibrational density of states spectra, visualization of the equilibration process and the order parameter, data from the SHAKE simulations, and local thermal conductivity figures (PDF)

■ AUTHOR INFORMATION

Corresponding Author

Jianying He − *Department of Structural Engineering, Norwegian University of Science and Technology (NTNU), Trondheim 7491, Norway;* orcid.org/0000-0001-8485-7893; Email: jianying.he@ntnu.no

Authors

Sandra Sæther − *Department of Structural Engineering, Norwegian University of Science and Technology (NTNU), Trondheim 7491, Norway;* orcid.org/0000-0001-9108-1368

Merete Falck − *Department of Structural Engineering, Norwegian University of Science and Technology (NTNU), Trondheim 7491, Norway*

Zhiliang Zhang − *Department of Structural Engineering, Norwegian University of Science and Technology (NTNU), Trondheim 7491, Norway;* orcid.org/0000-0002-9557-3455

Anders Lervik − *Department of Chemistry, Norwegian University of Science and Technology (NTNU), Trondheim 7491, Norway*

Complete contact information is available at: https://pubs.acs.org/10.1021/acs.macromol.1c00633

Notes

The authors declare no competing financial interest.

■ ACKNOWLEDGMENTS

This work is financially supported by the Research Council of Norway via HEFACE project (grant no. 251068). The computational resources are provided by Norwegian Metacenter for Computational Science (NOTUR NN9391k and NN9718k).

■ REFERENCES

(1) Xie, X.; Li, D.; Tsai, T.-H.; Liu, J.; Braun, P. V.; Cahill, D. G. Thermal conductivity, heat capacity, and elastic constants of water-soluble polymers and polymer blends. *Macromolecules* **2016**, *49*, 972−978.

(2) Shen, S.; Henry, A.; Tong, J.; Zheng, R.; Chen, G. Polyethylene nanofibres with very high thermal conductivities. *Nat. Nanotechnol.* **2010**, *5*, 251−255.

(3) Shulumba, N.; Hellman, O.; Minnich, A. J. Lattice thermal conductivity of polyethylene molecular crystals from first-principles including nuclear quantum effects. *Phys. Rev. Lett.* **2017**, *119*, 185901.

(4) Zhu, B.; Liu, J.; Wang, T.; Han, M.; Valloppilly, S.; Xu, S.; Wang, X. Novel polyethylene fibers of very high thermal conductivity enabled by amorphous restructuring. *ACS Omega* **2017**, *2*, 3931−3944.

(5) Lu, T.; Kim, K.; Li, X.; Zhou, J.; Chen, G.; Liu, J. Thermal transport in semicrystalline polyethylene by molecular dynamics simulation. *J. Appl. Phys.* **2018**, *123*, 015107.

(6) Xu, Y.; Kraemer, D.; Song, B.; Jiang, Z.; Zhou, J.; Loomis, J.; Wang, J.; Li, M.; Ghasemi, H.; Huang, X.; Li, X.; Chen, G. Nanostructured polymer films with metal-like thermal conductivity. *Nat. Commun.* **2019**, *10*, 1771.

(7) Henry, A.; Chen, G. High thermal conductivity of single polyethylene chains using molecular dynamics simulations. *Phys. Rev. Lett.* **2008**, *101*, 235502.

(8) He, J.; Kim, K.; Wang, Y.; Liu, J. Strain effects on the anisotropic thermal transport in crystalline polyethylene. *Appl. Phys. Lett.* **2018**, *112*, 051907.

(9) Xiong, X.; Yang, M.; Liu, C.; Li, X.; Tang, D. Thermal conductivity of cross-linked polyethylene from molecular dynamics simulation. *J. Appl. Phys.* **2017**, *122*, 035104.

(10) Muthaiah, R.; Garg, J. Temperature effects in the thermal conductivity of aligned amorphous polyethylene—A molecular dynamics study. *J. Appl. Phys.* **2018**, *124*, 105102.

(11) Zhang, T.; Luo, T. Morphology-influenced thermal conductivity of polyethylene single chains and crystalline fibers. *J. Appl. Phys.* **2012**, *112*, 094304.

(12) Ni, B.; Watanabe, T.; Phillpot, S. R. Thermal transport in polyethylene and at polyethylene−diamond interfaces investigated using molecular dynamics simulation. *J. Phys.: Condens. Matter* **2009**, *21*, 084219.

(13) Luo, C.; Kröger, M.; Sommer, J.-U. Entanglements and crystallization of concentrated polymer solutions: molecular dynamics simulations. *Macromolecules* **2016**, *49*, 9017−9025.

(14) Zhang, T.; Luo, T. Role of chain morphology and stiffness in thermal conductivity of amorphous polymers. *J. Phys. Chem. B* **2016**, *120*, 803−812.

(15) Rastgarkafshgarkolaei, R.; Zeng, Y.; Khodadadi, J. M. A molecular dynamics study of the effect of thermal boundary conductance on thermal transport of ideal crystal of n-alkanes with different number of carbon atoms. *J. Appl. Phys.* **2016**, *119*, 205107.

(16) Algaer, E. A.; Müller-Plathe, F. Molecular dynamics calculations of the thermal conductivity of molecular liquids, polymers, and carbon nanotubes. *Soft Mater.* **2012**, *10*, 42−80.

(17) Lussetti, E.; Terao, T.; Müller-Plathe, F. Nonequilibrium molecular dynamics calculation of the thermal conductivity of amorphous polyamide-6, 6. *J. Phys. Chem. B* **2007**, *111*, 11516−11523.

(18) Sirk, T. W.; Moore, S.; Brown, E. F. Characteristics of thermal conductivity in classical water models. *J. Chem. Phys.* **2013**, *138*, 064505.

(19) Rossinsky, E.; Müller-Plathe, F. Anisotropy of the thermal conductivity in a crystalline polymer: Reverse nonequilibrium molecular dynamics simulation of the δ phase of syndiotactic polystyrene. *J. Chem. Phys.* **2009**, *130*, 134905.

(20) Zhang, M.; Lussetti, E.; de Souza, L. E. S.; Müller-Plathe, F. Thermal conductivities of molecular liquids by reverse nonequilibrium molecular dynamics. *J. Phys. Chem. B* **2005**, *109*, 15060−15067.

(21) Chen, C.; Depa, P.; Sakai, V. G.; Maranas, J. K.; Lynn, J. W.; Peral, I.; Copley, J. R. D. A comparison of united atom, explicit atom, and coarse-grained simulation models for poly (ethylene oxide). *J. Chem. Phys.* **2006**, *124*, 234901.

(22) Chen, C.; Depa, P.; Maranas, J. K.; Garcia Sakai, V. Comparison of explicit atom, united atom, and coarse-grained simulations of poly (methyl methacrylate). *J. Chem. Phys.* **2008**, *128*, 124906.
(23) Li, C.; Choi, P.; Sundararajan, P. R. Simulation of chain folding in polyethylene: A comparison of united atom and explicit hydrogen atom models. *Polymer* **2010**, *51*, 2803−2808.
(24) Tenenbaum, A. Local equilibrium in stationary states by molecular dynamics. *Phys. Rev. A* **1983**, *28*, 3132−3133.
(25) Ikeshoji, T.; Hafskjold, B. Non-equilibrium molecular dynamics calculation of heat conduction in liquid and through liquid-gas interface. *Mol. Phys.* **1994**, *81*, 251−261.
(26) Römer, F.; Lervik, A.; Bresme, F. Nonequilibrium molecular dynamics simulations of the thermal conductivity of water: A systematic investigation of the SPC/E and TIP4P/2005 models. *J. Chem. Phys.* **2012**, *137*, 074503.
(27) Luo, T.; Esfarjani, K.; Shiomi, J.; Henry, A.; Chen, G. Molecular dynamics simulation of thermal energy transport in polydimethylsiloxane. *J. Appl. Phys.* **2011**, *109*, 074321.
(28) Hafskjold, B.; Ratkje, S. K. Criteria for local equilibrium in a system with transport of heat and mass. *J. Stat. Phys.* **1995**, *78*, 463−494.
(29) Plimpton, S. Fast Parallel Algorithms for Short-Range Molecular Dynamics. *J. Comput. Phys.* **1995**, *117*, 1−19.
(30) Jorgensen, W. L.; Tirado-Rives, J. The OPLS [optimized potentials for liquid simulations] potential functions for proteins, energy minimizations for crystals of cyclic peptides and crambin. *J. Am. Chem. Soc.* **1988**, *110*, 1657−1666.
(31) Olsson, P. A. T.; in't Veld, P. J.; Andreasson, E.; Bergvall, E.; Persson Jutemar, E.; Petersson, V.; Rutledge, G. C.; Kroon, M. All-atomic and coarse-grained molecular dynamics investigation of deformation in semi-crystalline lamellar polyethylene. *Polymer* **2018**, *153*, 305−316.
(32) Jorgensen, W. L.; Maxwell, D. S.; Tirado-Rives, J. Development and testing of the OPLS all-atom force field on conformational energetics and properties of organic liquids. *J. Am. Chem. Soc.* **1996**, *118*, 11225−11236.
(33) Paul, W.; Yoon, D. Y.; Smith, G. D. An optimized united atom model for simulations of polymethylene melts. *J. Chem. Phys.* **1995**, *103*, 1702−1709.
(34) Ryckaert, J.-P.; Ciccotti, G.; Berendsen, H. J. C. Numerical integration of the cartesian equations of motion of a system with constraints: molecular dynamics of *n*-alkanes. *J. Comput. Phys.* **1977**, *23*, 327−341.
(35) Lee, S.; Rutledge, G. C. Plastic deformation of semicrystalline polyethylene by molecular simulation. *Macromolecules* **2011**, *44*, 3096−3108.
(36) Kim, J. M.; Locker, R.; Rutledge, G. C. Plastic deformation of semicrystalline polyethylene under extension, compression, and shear using molecular dynamics simulation. *Macromolecules* **2014**, *47*, 2515−2528.
(37) Meyer, H.; Müller-Plathe, F. Formation of chain-folded structures in supercooled polymer melts. *J. Chem. Phys.* **2001**, *115*, 7807−7810.
(38) Luo, C.; Sommer, J.-U. Frozen topology: Entanglements control nucleation and crystallization in polymers. *Phys. Rev. Lett.* **2014**, *112*, 195702.
(39) Anwar, M.; Schilling, T. Crystallization of polyethylene: A molecular dynamics simulation study of the nucleation and growth mechanisms. *Polymer* **2015**, *76*, 307−312.
(40) Jabbari-Farouji, S.; Lame, O.; Perez, M.; Rottler, J.; Barrat, J.-L. Role of the intercrystalline tie chains network in the mechanical response of semicrystalline polymers. *Phys. Rev. Lett.* **2017**, *118*, 217802.
(41) Moyassari, A.; Gkourmpis, T.; Hedenqvist, M. S.; Gedde, U. W. Molecular dynamics simulation of linear polyethylene blends: Effect of molar mass bimodality on topological characteristics and mechanical behavior. *Polymer* **2019**, *161*, 139−150.
(42) in't Veld, P. J.; Rutledge, G. C. Temperature-dependent elasticity of a semicrystalline interphase composed of freely rotating chains. *Macromolecules* **2003**, *36*, 7358−7365.
(43) Peacock, A. J. *Handbook of Polyethylene: Structures: Properties, and Applications*; CRC press, 2000.
(44) Bates, M. A.; Frenkel, D. Phase behavior of two-dimensional hard rod fluids. *J. Chem. Phys.* **2000**, *112*, 10034−10041.
(45) Virtanen, P.; et al. SciPy 1.0: Fundamental Algorithms for Scientific Computing in Python. *Nat. Methods* **2020**, *17*, 261−272.
(46) Choy, C. L. Thermal conductivity of polymers. *Polymer* **1977**, *18*, 984−1004.
(47) Hansen, D.; Bernier, G. A. Thermal conductivity of polyethylene: The effects of crystal size, density and orientation on the thermal conductivity. *Polym. Eng. Sci.* **1972**, *12*, 204−208.
(48) Zeng, Y.; Dong, J.; Khodadadi, J. M. Thermal coupling-decoupling mechanism of heat transfer across van der Waals interfaces in n-eicosane. *Int. J. Heat Mass Transfer* **2021**, *164*, 120603.
(49) Duan, X.; Li, Z.; Liu, J.; Chen, G.; Li, X. Roles of kink on the thermal transport in single polyethylene chains. *J. Appl. Phys.* **2019**, *125*, 164303.
(50) Hu, M.; Shenogin, S.; Keblinski, P. Molecular dynamics simulation of interfacial thermal conductance between silicon and amorphous polyethylene. *Appl. Phys. Lett.* **2007**, *91*, 241910.

https://doi.org/10.1021/acs.macromol.1c00633
Macromolecules 2021, 54, 6563−6574